

# Progress in characterizing submonolayer island growth: Capture-zone distributions, growth exponents, & hot precursors

Theodore L. Einstein<sup>1,2</sup>, Alberto Pimpinelli<sup>1,3</sup>, Diego Luis González<sup>1,4</sup>, Josue R. Morales-Cifuentes<sup>1,2</sup>

<sup>1</sup>Dept. Physics & <sup>2</sup>CMTC, University of Maryland, College Park, MD 20742-4111 USA

<sup>3</sup>Rice Quantum Institute & MSNE Department, Rice University, Houston, TX 77005 USA

<sup>4</sup>Departamento de Física, Universidad del Valle, A.A. 25360, Cali, Colombia

E-mail: einstein@umd.edu; ap19@rice.edu; diego.luis.gonzalez@correounivalle.edu.co

**Abstract.** In studies of epitaxial growth, analysis of the distribution of the areas of capture zones (i.e. proximity polygons or Voronoi tessellations with respect to island centers) is often the best way to extract the critical nucleus size  $i$ . For non-random nucleation the normalized areas  $s$  of these Voronoi cells are well described by the generalized Wigner distribution (GWD)  $P_\beta(s) = as^\beta \exp(-bs^2)$ , particularly in the central region  $0.5 < s < 2$  where data are least noisy. Extensive Monte Carlo simulations reveal inadequacies of our earlier mean field analysis, suggesting  $\beta = i + 2$  for diffusion-limited aggregation (DLA). Since simulations generate orders of magnitude more data than experiments, they permit close examination of the tails of the distribution, which differ from the simple GWD form. One refinement is based on a fragmentation model. We also compare island-size distributions. We compare analysis by island-size distribution and by scaling of island density with flux. Modifications appear for attach-limited aggregation (ALA). We focus on the experimental system *para*-hexaphenyl on amorphous mica, comparing the results of the three analysis techniques and reconciling their results via a novel model of hot precursors based on rate equations, pointing out the existence of intermediate scaling regimes between DLA and ALA.

## 1. Introduction

During the last decade several fine reviews [1, 2, 3, 4] have been published about the early stages of thin-film growth. In this aggregation regime a major goal is to assess the size of the smallest stable cluster (denoted  $i+1$ , where  $i$  is the size of the critical nucleus, the largest unstable cluster [5, 6, 7, 8]). Three approaches have been taken in this pursuit: 1) rate equation theory for the scaling, with incident flux  $F$ , of island density  $N \propto F^{\alpha_i}$ ; 2) analysis of the island-size distribution (ISD); and most recently 3) analysis of the capture-zone distribution (CZD). For ICCGE17 we recently prepared a minireview of these investigations [9], emphasizing the CZD approach. Here we include some highlights of that paper but with emphasis on a single experimental system, *para*-hexaphenyl (6P) on sputter-amorphized mica, showing results relevant to all three approaches and describing how including the participation of hot precursors reconciles the scaling data with the CZD and ISD results [10].

## 2. Capture-Zone Distributions and the Generalized Wigner Distribution

We begin with the most recent approach, the distribution of the areas of capture zones [3, 11, 12, 13], i.e. Voronoi (proximity) cells constructed from the islands. Cf. Fig. 1a,b. This



CZD turns out to provide information about  $i$ . For the Poisson-Voronoi (PV) case of random nucleation centers, the CZD is expected to follow a gamma distribution  $P_{\Gamma}^{(a)}(s)$  [14, 15],

$$P_{\Gamma}^{(a)}(s) = \frac{a^a}{\Gamma(a)} s^{a-1} e^{-as}, \quad (1)$$

where  $s$  is the CZ area divided by its average value (so that  $\langle s \rangle = 1$ ).

More generally we have argued [13], drawing from experiences analyzing the terrace-width distributions of vicinal surfaces [17], that the CZD is better described by the single-parameter generalized Wigner distribution (GWD):

$$P_{\beta}(s) = a_{\beta} s^{\beta} e^{-b_{\beta} s^2}, \quad a_{\beta} = 2\Gamma\left(\frac{\beta+2}{2}\right)^{\beta+1} / \Gamma\left(\frac{\beta+1}{2}\right)^{\beta+2}, \quad b_{\beta} = \left[ \Gamma\left(\frac{\beta+2}{2}\right) / \Gamma\left(\frac{\beta+1}{2}\right) \right]^2, \quad (2)$$

where  $a_{\beta}$  and  $b_{\beta}$  are dictated by normalization and unit mean, respectively, of  $P_{\beta}(s)$ . Our derivation of  $P_{\beta}(s)$  from a mean-field Fokker-Planck equation implied that  $\beta = i + 1$  in two dimensions (2D) [13].

Extensive simulations exposed inadequacies of this mean-field prediction [18], ultimately because nucleation occurs preferentially near CZ boundaries rather than uniformly [19, 20], so that in 2D  $\beta = i + 2$  (for *diffusion-limited aggregation* (DLA)) is better. Shi et al. [21] performed kinetic Monte Carlo calculations of irreversible growth ( $i = 1$ ) of point islands with dimensions 1–4, for both square and triangular lattices in 2D and for two different point-island models. They used values of  $R = 10^5 - 10^{10}$ , where  $R \equiv D/F$ ,  $D$  the diffusion rate and  $F$  the deposition flux, in order to extrapolate to asymptotic behavior. Their fits to CZDs are better with  $\beta = 3$  than with  $\beta = 2$ . While the coverage dependence (between 0.1 and 0.4 ML) is negligible, there is some dependence on  $R$  and on which of the two models of point islands is used. They also find better scaling (with  $R$ ) of the peak height of the CZD using  $\beta = 3$ , and comparable results for the two models. Li et al. [19] considered both  $i = 1$  and  $i = 0$  at 0.1 ML, finding that  $\beta = 3$  accounts better for their  $i = 1$  CZD curve than  $\beta = 2$ . The GWD describes the CZD over the values of  $s$  for which there is significant data in experiments ( $0.5 < s < 2$ ) but has deficiencies in the tails at high and low  $s$  [19, 22]. For large  $s$ ,  $P(s)$  may decay exponentially or like a generalized gamma distribution  $s^{\beta\nu} \exp(-\text{const.} \cdot s^{\nu})$  (with non-integer  $\nu$ ) rather than in Gaussian fashion. Thus, their best fit gives  $\nu = 1.5$  and  $\beta_{\nu} \approx 4$  (and  $\nu = 1.3$  and  $\beta_{\nu} \approx 3$  for  $i = 0$ ). However, the relation between  $\beta$  and  $i$  should be determined by the central part of the CZD rather than power-law behavior for  $s \ll 1$ , so that  $\beta_{\nu}$  and  $\beta$  are expected to differ; i.e.,  $\beta$

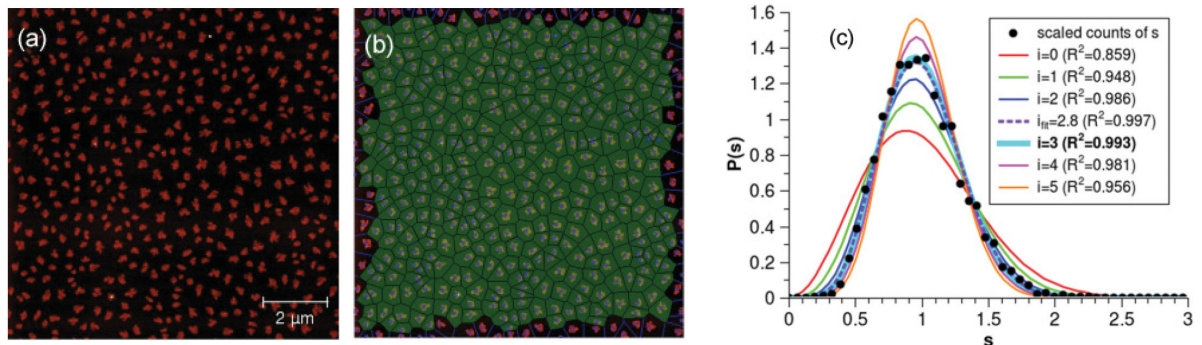


**Figure 1.** (a) Islands of standing *para*-hexaphenyl (6P) on sputtered mica (001) at 0.19 ML,  $T = 300\text{K}$ ,  $F = 0.04$  ML/min. (b) Construction of capture zones of (a) by Voronoi tessellation. (c) Resulting CZD from (b) compared with  $P_{\beta}(s)$  for  $\beta = 2-7$  ( $i = \beta - 2$  for DLA). From [16].

is essentially an effective exponent. (Furthermore,  $\beta_\nu$  increases to “compensate” decreasing  $\nu$ . The non-Gaussian decay stems from the probability  $\sim s^\nu$  that a new CZ overlaps an existing CZ of scaled area  $s$  [3, 23];  $\nu$  is typically extracted from numerical data.)

Most recently Oliveira and Aarão Reis [22] reported extensive simulations in 2D for point and extended (fractal and square) islands, with  $i = 1$  and 2, for  $R = 10^6 - 10^{10}$ . Rather than using  $s$  as their independent (scaling) variable, they choose  $u = (x - \langle x \rangle) / \sigma_x \rightarrow (s-1)[(\beta+1)/(2b_\beta)-1]^{-1/2}$ , where  $x$  is the number of lattice sites within a CZ, and  $\sigma_x$  is the standard deviation; the final expression for  $u$  is its form for the GWD. This scaling procedure improves data collapse (for different values of  $R$ ) by reducing the corrections to scaling for small  $x$ , where the continuum model underlying the derivation of Eq. (2) becomes inaccurate. However, this scaling obscures the variation of the curves with changing values of  $i$  (and so  $\beta$ ) in the central region [9] (but brings out differences in the tails in their log-linear plots). For point islands with  $i = 1$ ,  $\beta = 2$  and 3 both give “good fits” in the central (peak) region, with  $\beta = 3$  also adequate for small  $s$  and neither doing well for large  $s$ ; for  $i = 2$ ,  $\beta = 3$  fits well the center and large- $s$  tail. For fractal and for square islands,  $\beta = i + 1$  gives a good fit for four values of  $R$ , while  $\beta = i + 2$ , though not mentioned [22]a, is also satisfactory [22]d. Typically there is Gaussian decay for large  $s$ .

While the numerical studies leave some open questions, the preponderance of evidence points to  $\beta \approx i + 2$ , which we can retrieve by refining our derivation [24]: Noting that within a circular zone of radius  $r_0$ , the adatom density  $n(r) \propto r_0^2 - r^2$ , so that the integral over CZ area of  $[n(r)]^{i+1} \propto r_0^{2i+4} \Rightarrow P(s) \propto s^{i+2}$ . Furthermore, experimental data well described by  $P_\beta(s)$  can also be fit with  $P_\Gamma^{(a \approx 2\beta+1)}(s)$  [25], progressively better for larger exponents [9].

In a refined analysis based on a widely-applicable *fragmentation model* (FM) [12], we characterized systems in terms of two physically-rooted exponents,  $\gamma$  and  $\delta$  [20], by taking (a) the probability to nucleate, in a cell of size  $s$ ,  $\propto s^\gamma P(s)$ , ultimately, implying  $P(s) \sim \exp(-\text{const.}s^\gamma)$  for  $s \gg 1$ ; and (b) the probability that a new center lies at a position  $\mathbf{r}$ , relative to the center of a preexisting cell,  $\propto |\mathbf{r}|^\delta$ , assuming circular isotropy for simplicity. The simplest case is the PV problem, for which  $\gamma = 1$  and  $\delta = 0$ , with the second probability  $\mathbf{r}$ -independent but  $\propto s^{-1}$  [20].

A harder but still tractable example is a point-island model, with irreversible attachment, in which capture zones are approximated as circular [20]. The isotropic solution of the appropriate steady-state diffusion equation gives an adatom density  $n(\rho)$  that increases from 0 at the interior island edge to a smooth maximum at the outer edge. Thence we deduce that  $\gamma = 3$  (more generally  $\gamma = i + 2$ ), which, with  $\delta = 0$ , accounts adequately for numerical data for  $P(s)$ , but less well for island density and the radial nearest-neighbor island probability distribution. This deficiency can be remedied by taking  $\delta = 1$  near the center and  $\delta = 0$  near the edge [20]. In the FM the above-noted result  $\nu = 1.5$  [19] implies  $\gamma = 1.5$ , with  $\delta \approx 1.2$  near the center and  $\delta = 0$  near the edge [20]. Furthermore, the above mean-field-based argument for  $\gamma = 3$  overestimates  $\gamma$ , which extensive simulations show to be close to 2 rather than 3 at low coverages and large  $R$ .

For  $s \ll 1$ ,  $P(s)$  is expected to behave like a power law in  $s$ , but the precise relation between this exponent and  $i$  has not yet been determined, although for  $i = 1$  good agreement with simulations has been found for the (actual rather than effective) exponent  $\beta = 4$  [19, 20, 22]. In this regime  $P(s)$  depends on the concentration of centers and ultimately, in the FM model, on  $\delta$  [20]. The skewness of the GWD also agrees well with numerical data in simulations [22]. However, earlier efforts to fit experimental data by just extracting the first few moments of the distribution were unsatisfactory [26]. Alternatively, one can allow two different values of  $\gamma$ : 2 for small  $s$  and 1 for large  $s$ . While such a “two-regime model” is not essential in 2D, it is in 1D. For the detailed analyses and controversies in the 1D case, see [12, 19, 20, 21, 22, 27, 28].

### 3. Island Size Distributions and Scaling of Island Number vs. Flux

Two alternative approaches have long been used to gauge the critical nucleus size from experiment. One is to measure the island size distribution (ISD) [3, 29, 30] and then to fit

it with the Amar-Family scaling formula (at least for  $i = 1,2,3$  and in 2D) [31],

$$f_i(u) = C_i u^i e^{-ia_i u^{1/a_i}}, \quad \frac{\Gamma[(i+2)a_i]}{\Gamma[(i+1)a_i]} = (ia_i)^{a_i}; \quad f(u) \underset{R \rightarrow \infty}{=} f(0) \exp \left[ \int_0^u dy \frac{2z-1-C'_{\text{tot}}(y)}{C_{\text{tot}}(y)-zy} \right], \quad (3)$$

with  $u$  now the island size divided by its mean and  $C_i$  a normalization constant; Amar et al. deduced  $f_i(u)$  empirically from the expectations that (in the limit of large  $R$ )  $f_i$  goes like  $u^i$  for small  $u$ , cuts off exponentially for large  $u$ , and peaks at  $u = 1$  (unlike the GWD, which peaks at  $u < 1$ , especially noticeable for small  $\beta$ ). With scaling assumptions for capture numbers and neglect of deposition dependence, Bartelt and Evans [3, 23, 32] obtained the  $R \rightarrow \infty$  limit, where  $C_{\text{tot}}$  is a linear combination of scaled capture numbers and capture zones and  $z$  is the slope of a log-log plot of mean island size vs.  $F$  (e.g.,  $z = 2/3$  for point islands). In principle, then, the ISD can be obtained from a rate-equation approach if one has information about the capture numbers [1, 32]; they can be measured from simulations since calculating them is intractable.

While the ISD does not generally mimic the CZD [3, 33], kinetic Monte Carlo (KMC) calculations by Fanfoni et al. on a simple model of quantum dot growth reveal a similarity between ISD and CZD at lower temperature  $T$ , when evolution of islands is dominated by atom motion along the periphery rather than attachment/detachment [34]. (However, they favor the  $P_{\Gamma}^{(a)}(s)$  over  $P_{\beta}(s)$  in their fits.) See [22] for recent results on the high-end tails.

The second approach, based on rate equation theory, involves the scaling of the density  $N$  of [stable] islands (particularly the maximum density) with  $F$ : it is long known [5, 6] that at constant, relatively low  $T$ , there is the scaling relation [6, 35]

$$N \sim F^{\alpha_i} \exp(E_i / [(i+2)k_B T]), \quad \alpha_i^{\text{DLA}} = i / (i+2), \quad \alpha_i^{\text{ALA}} = 2i / (i+3) \quad (4)$$

where  $E_i$  is the cohesion energy of a cluster of size  $i$ . The two relations of  $\alpha_i$  to  $i$  are DLA and attachment-limited aggregation (ALA) regimes [36] in 2D, respectively. There are many other regimes with signature relations for  $\alpha_i$  [35, 37, 10]. Also, the values in 3D differ, e.g. being  $2i / (2i + 5)$  for DLA (with compact islands and with no desorption). In short, the value of  $i$  deduced from  $\alpha_i$  depends strongly on the dominant mode of mass transport. In many cases one can characterize the  $T$  dependence by writing  $N \sim (F/D)^{\alpha_i}$ , where  $D$  has an activated, Arrhenius form; then the ‘‘activation energy’’ is enhanced by a term proportional to the diffusion barrier. Thus,  $N$  is expected to decrease rapidly with increasing  $T$  [8]. While a great deal of information can be gleaned from this characteristic energy, or its effective generalization  $d \ln N / d(1/k_B T)$ , space precludes a detailed discussion here; readers should consult [6, 7, 8, 10].

#### 4. Experimental Applications: *Para*-hexaphenyl on Sputter-Amorphized Mica

In [9] we provided capsule descriptions of the many experimental applications of CZD analysis; here we simply give a list: pentacene on  $\text{SiO}_2$  [38], pentacene with controlled pentacenequinone impurities [39], polar-conjugated molecule  $\text{Alq}_3$  on passivated  $\text{Si}(100)$  [40], self-assembled  $\text{Ge}/\text{Si}(001)$  nanoislands [41],  $\text{InAs}$  quantum dots on  $\text{GaAs}(001)$  [34, 42], metallic Ga droplets on  $\text{GaAs}(001)$  [43],  $\text{C}_{60}$  on UTO [25], 6P on  $\text{Ir}(111)$ , 6P on  $\text{SiO}_2$  [44], and 6P films on amorphous mica [16, 45, 46, 47, 48]. Here we concentrate on the last in this list, to which all three approaches have been applied. Note that interest in rod-like 6P is spurred in part by its use in blue-light-emitting diodes [49], nano-optic devices [50], etc. We show that all three methods give values of  $i$  that are reasonably consistent with one other, notwithstanding some reported values.

The sample image in Fig. 1a is of islands of 6P for 0.19 ML,  $T = 300\text{K}$ , and  $F = 0.04$  ML/min on freshly cleaved muscovite mica (001), sputter-modified to ensure the 6P are all standing, thereby precluding a competing wetting layer [16]. The Voronoi tessellation of such images, as in Fig. 1b, is used to tally the CZD. Fig. 1c then shows that the CZD is well (and

best) fit with  $\beta = 5$ , leading to  $i = 3$  (within the assumption of DLA). Fig. 2a depicts the ISD for these islands again at  $T = 300\text{K}$  but with half the flux. Based on a least-squares fit to Eq. (3), the result is again  $i = 3 \pm 1$ . Subsequently this group [46] found that this ISD is for large and rather dendritic islands; they report  $i = 2$ , but given the modest amount of data, this is viewed as consistent with the earlier value. (There are also smaller, compact islands with a smaller critical nucleus size,  $i = 1$ .) Third, Winkler’s group’s analysis of  $N(F)$  data at 300K with Eq. (4) with  $\alpha_i = i/(i+2)$  yielding  $i = 2.5 \pm 0.5$  [16]. For such small  $i$  they conclude that the 6P molecules must be lying on the surface, rather than standing up. Assuming DLA and ALA Different behavior is found at low  $T$ , attributable to different kinetics [16]. Subsequent work on sputtered mica [45] showed that the 6P molecules stand up, suggesting a higher  $i$ . While no CZD analysis is given, values of  $\alpha_i$  in both the DLA and the ALA regimes give  $i = 7 \pm 2$  [51].

For pentacene on sputter-amorphized mica at 300 K, there is similar dogleg behavior in the plot of  $\ln N$  vs.  $\ln F$ , with  $\alpha = 0.8 \pm 0.1$  and  $\alpha = 1.3 \pm 0.1$ [48]. Using Eq. (4) they deduce  $i = 5 \pm 1$ . For the CZD they found  $\beta = 5.0 \pm 0.5$  and  $\beta = 4.0 \pm 0.5$  for  $F = 0.08$  and 1.37 ML/min., respectively, at 300K. They deduce  $\alpha\beta \approx i$  globally, with the noteworthy corollary  $\beta_{\text{ALA}} = (i+3)/2$ .

### 5. Hot Precursor Model

Very recently three of us presented a model, formulated in terms of rate equations, that treats the modification of island nucleation by “hot precursors,” i.e., deposited molecules which propagate ballistically for some distance before thermalizing or joining an island [10]. A key dimensionless parameter is  $z \equiv \tau_h/\tau_{h \rightarrow N}$ , the ratio of the thermalization time to the hot-precursor survival time before capture by an island. For  $z \ll 1$  and  $z \gg 1$ , i.e. fast and slow thermalization, we recover, respectively, DLA and a novel hot monomer aggregation (HMA) regime with  $\alpha$  the same as for ALA. However, the crossover between these regimes is not a smooth monotonic crossover. Two other dimensionless terms come into play, the ratio  $\mathcal{R}_n$  of hot to thermalized monomers and a ballistic scale  $\mathcal{R}_B$  related to the distance hot monomers travel to the spacing between islands). (A third ratio, expressing whether ballistic or thermalized channels dominate decay, also plays

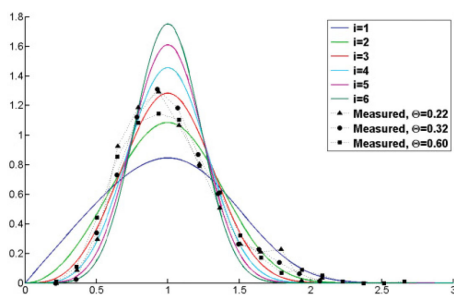


**Figure 2.** ISD for 6P islands vs. normalized area  $s$ , after deposition of three different coverages ( $\Theta = 0.22, 0.32$ , and  $0.60\text{ML}$ ) at 300K with  $F = 0.02$  ML/min, measured with *ex situ* AFM at room temperature. The island density is scaled by  $\langle s \rangle^2/\Theta$ . The least-squares best fit using Eq. (3) yields  $i = 3 \pm 1$ . From Fig. 2 of [16] A similar plot with less data in Fig. 10a of [46] for 0.147 ML at 400K reports  $i = 2$ .

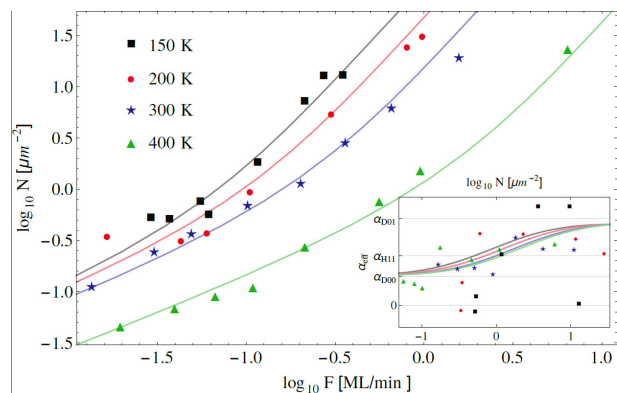


**Figure 3.** Island density vs. deposition rate in the aggregation regime for 6P on sputter-modified mica (001) [45] at  $T = 150\text{K}$  (black, square dots), 200K (red, round dots), 300K (blue, star dots), and 400K (green, triangular dots), with  $i = 4$  and several other dimensionless best-fit parameters given in [10]. Inset:  $\alpha_{\text{eff}}$  (curves) and values of  $d \ln N/d \ln F$  from the experimental data (dots). Adapted from Fig. 3 of [10]

a role if we consider the effective activation energy.) In plots of the effective  $\alpha \equiv d \ln N / d \ln F$  vs.  $z$ , one finds the expected flat regions for small (DLA) and large (HMA/ALA)  $z$  but the expected non-monotonic crossover with extended plateaus corresponding to extreme values of  $\mathcal{R}_n$  and  $\mathcal{R}_B$ . (See Fig. 1 of [10].) Likewise, there are such plateaus for the effective activation energy. As a test of this model, we used the solution of the rate-equation formulation to fit simultaneously data for four temperatures, as shown in Fig. 3, with the result  $i = 4 \pm 1$  rather than  $i = 7 \pm 2$ . While the data at small  $z$  does correspond to DLA, that at high  $z$  is not ALA but rather the case of small  $z$  and  $\mathcal{R}_n$  but large  $\mathcal{R}_B$ , for which  $\alpha = i/2$  rather than  $2i/(i+3)$ .

## 6. Conclusions

We have discussed the three methods to investigate the critical nucleus size in submonolayer growth. For the case of 6P on amorphous mica, we found that scaling of island density gives results consistent with CZD analysis, once hot precursors are properly taken into account, showing the importance of that mechanism. We have shown that the GWD provides an excellent accounting of CZDs in the region where the data in experiments is most reliable. While the fits with  $P_{\Gamma}^{(n)}(s)$  (or even a Gaussian, for large  $\beta$ ) may also be adequate, only the GWD offers a fundamental connection  $\beta \approx i + 2$ . Further improvements in the theory, notably the fragmentation model, allow more detailed examination of tails and of other statistical functions. We have also applied CZD analysis to data from homoepitaxial growth on vicinal Cu(001), finding that codeposited impurities offer the most likely explanation of the data [52]. The approach applies to a much broader range of problems than just crystal growth: we have characterized the distribution of Metro stations in central Paris [20] and of the areas of secondary administrative units (counties in the USA, *arrondissements* in France, etc.) [20, 53].

## Acknowledgments

Work at UMD currently supported by NSF Grant No. CHE 13-05892. We are grateful for collaborations on CZD analysis with theorists R. Sathiyarayanan and A. BH. Hammouda, with the UMD experimental surface physics group, especially E.D. Williams, W.G. Cullen, B.R. Conrad, and M.A. Groce, and on scaling in growth with A. Winkler and his group at Graz.

## References

- [1] Ratsch C and Venables J A 2003 *J. Vac. Sci. Tech. A* **21** S96
- [2] Michely T and Krug J 2004 *Islands, Mounds and Atoms: Patterns and Processes in Crystal Growth Far from Equilibrium* (Berlin: Springer)
- [3] Evans J W, Thiel P A and Bartelt M C 2006 *Surf. Sci. Rep.* **61** 1
- [4] Einax M, Dieterich W and Maass P 2013 *Rev. Mod. Phys.* **85** 921
- [5] Stowell M 1970 *Phil. Mag.* **21** 125
- [6] Venables J A, Spiller G D and Hanbücken M 1984 *Rep. Prog. Phys.* **47** 399, and references therein
- [7] Brune H 1998 *Surf. Sci. Rep.* **31** 121
- [8] Pimpinelli A and Villain J 1998 *Physics of Crystal Growth* (Cambridge: Cambridge University Press)
- [9] Einstein T L, Pimpinelli A and D. L. González D L 2014 *J. Cryst. Growth* **401** 627
- [10] Morales-Cifuentes J R, Einstein T L and Pimpinelli A 2014 *Phys. Rev. Lett.* **113** 246101; arXiv 1411.6575
- [11] Mulheran P A and Blackman J A 1995 *Philos. Mag. Lett.* **72** 55; 1996 *Phys. Rev. B* **53** 10261
- [12] Blackman J A and P. A. Mulheran P A 1996 *Phys. Rev. B* **54** 11681
- [13] Pimpinelli A and Einstein T L 2007 *Phys. Rev. Lett.* **99** 226102
- [14] Kiang T 1966 *Z. Astrophysik* **64** 433
- [15] Ferenc J S and Z. Néda Z 2007 *Physica A* **385** 518
- [16] Potocar T, Lorbek G, Nabok D et al. 2011 *Phys. Rev. B* **83** 075423
- [17] Einstein T L and Pierre-Louis O 1999 *Surface Sci.* **424** L299; Einstein T L 2007 *Appl. Phys. A* **87** 375
- [18] Mean field works better in 1D, but that case requires—and permits—a more complicated analysis [12, 27, 28]
- [19] Li M, Han Y and Evans J W 2010 *Phys. Rev. Lett.* **104** 149601
- [20] González D L and Einstein T L 2011 *Phys. Rev. E* **84** 051135
- [21] Shi F, Shim Y and Amar J G 2009 *Phys. Rev. E* **79** 011602

- [22] Oliveira T J and Aarão Reis F D A, a) 2011 *Phys. Rev. B* **83** 201405; b) 2012 **86** 115402; c) 2013 **87** 235430; d) Aarão Reis F D A, private communication, 2014
- [23] Bartelt M C and Evans J W 1996 *Phys. Rev. B* **54** 17359R; 2001 **63** 235408; 2002 **66** 235410
- [24] Pimpinelli A and Einstein T L 2010 *Phys. Rev. Lett.* **104** 49602
- [25] Groce M et al. 2012 *Surface Sci.* **606** 53; Michelle A. Groce, Ph.D. dissertation, University of Maryland, 2013; <http://search.proquest.com/docview/1464775310>
- [26] Giesen M and Einstein T L 2000 *Surface Sci.* **449** 191
- [27] González D L, Pimpinelli A and Einstein T L 2011 *Phys. Rev. E* **84** 011601.
- [28] Grinfeld M et al. 2012 *J. Phys. A: Math. Theor.* **45** 015002; O'Neill K P et al. 2012 *Phys. Rev. E* **85** 021601; Mulheran P A et al. 2012 *Phys. Rev. E* **86** 051606
- [29] Amar J G, Family F and Lam P M 1994 *Phys. Rev. B* **50** 8781
- [30] Bartelt M C and Evans J W 1992 *Phys. Rev. B* **46** 12675; Ratsch C et al. 1994 *Phys. Rev. Lett.* **72** 3194
- [31] Amar J G and F. Family F 1995 *Phys. Rev. Lett.* **74** 2066
- [32] Körner M, Einax M and Maass P 2010 *Phys. Rev. B* **82** 201401(R); 2012 *Phys. Rev. B* **86** 085403
- [33] P. A. Mulheran P A and Robbie D A 2000 *Europhys. Lett.* **49** 617
- [34] Fanfoni M, Arciprete F, Tirabassi C et al. 2012 *Phys. Rev. E* **86** 061605
- [35] Pimpinelli A, Jensen P, Larralde H and Peyla P 1998, in *Morphological Organization in Epitaxial Growth and Removal*, ed Z Zhang and M G Lagally (Singapore: World Scientific) p 121
- [36] Kandel D 1997 *Phys. Rev. Lett.* **78** 499
- [37] Pimpinelli A, Larralde H and Jensen P 1997 *Phys. Rev. B* **55** 2556
- [38] Pratontop S, Brinkmann M, Nüesch F and Zuppiroli L 2004 *Phys. Rev. B* **69** 165201
- [39] Conrad B R, Gomar-Nadal E, Cullen W G et al. 2008 *Phys. Rev. B* **77** 205338
- [40] Brinkmann M, Graff S and Biscarini F 2002 *Phys. Rev. B* **66** 165430
- [41] Miyamoto S, Moutanabbir O, Haller E E and Itoh K M 2009 *Phys. Rev. B* **79** 165415
- [42] a) Fanfoni M et al. 2007 *Phys. Rev. B* **75** 245312; b) Placidi E et al. 2007 *J. Phys. Cond. Mat.* **19** 225006
- [43] Nothorn D M and Millunchick J M 2007 *J. Vac. Sci. Tech. B* **30** 060603
- [44] Lorbek S, Hlawacek G and Teichert C 2011 *Eur. Phys. J. Appl. Phys.* **55** 23902
- [45] Tumbek L and Winkler A 2012 *Surface Sci.* **606** L55
- [46] Tumbek L, Gleichweit C, Zojer K and Winkler A 2012 *Phys. Rev. B* **86** 085402
- [47] Winkler A and Tumbek L 2013 *J. Chem. Phys. Lett.* **4** 4080
- [48] Pimpinelli A, Tumbek L and Winkler A 2014 *J. Phys. Chem. Lett.* **5** 995
- [49] Yanagi H and Okomato S 1997 *Appl. Phys. Lett.* **71** 2563
- [50] Balzer F and Rubahn H G 2005 *Adv. Funct. Mater.* **15** 17
- [51] Hlawacek G, Khokar F S, van Gastel R, Teichert C and Poelsema B 2011 *IBM J. Res. & Dev.* **55** 15
- [52] Hamouda A BM et al. 2011 *Phys. Rev. B* **83** 035423; Sathiyarayanan R et al. 2011 *Phys. Rev. B* **83** 035424
- [53] Rajesh Sathiyarayanan, Ph.D. thesis, Maryland, 2009; <http://pqdtopen.proquest.com/doc/304923517.html?FMT=ABS>; Sathiyarayanan R et al., preprint